Crystal Structure at 2.5 Å Resolution of Zinc-Substituted Copper Amine Oxidase of *Hansenula polymorpha* Expressed in *Escherichia coli*[†,‡]

Zhi-wei Chen,[§] Benjamin Schwartz,[||] Neal K. Williams,[||,⊥] Rongbao Li,[§,#] Judith P. Klinman,[||] and F. Scott Mathews*[,§]

Department of Biochemistry and Molecular Biophysics, Washington University School of Medicine, St. Louis, Missouri 63110, and Departments of Chemistry and Molecular and Cell Biology, University of California, Berkeley, California 94720

Received March 20, 2000; Revised Manuscript Received May 8, 2000

ABSTRACT: Copper amine oxidases (CAOs) catalyze the two-electron oxidation of primary amines to aldehydes, utilizing molecular oxygen as a terminal electron acceptor. To accomplish this transformation, CAOs utilize two cofactors: a mononuclear copper, and a unique redox cofactor, 2,4,5-trihydroxyphenylalanine quinone (TPQ or TOPA quinone). TPQ is derived via posttranslational modification of a specific tyrosine residue within the protein itself. In this study, the structure of an amine oxidase from *Hansenula polymorpha* has been solved to 2.5 Å resolution, in which the precursor tyrosine is unprocessed to TPQ, and the copper site is occupied by zinc. Significantly, the precursor tyrosine directly ligands the metal, thus providing the closest analogue to date of an intermediate in TPQ production. Besides this result, the rearrangement of other active site residues (relative to the mature enzyme) proposed to be involved in the binding of molecular oxygen may shed light on how CAOs efficiently use their active site to carry out both cofactor formation and catalysis.

Copper-containing amine oxidases (CAOs,[1] EC 1.4.3.6) catalyze the two-electron oxidation of primary amines to the corresponding aldehydes, utilizing molecular oxygen as the terminal electron acceptor (eq 1) (*1*−*3*):

$$RCH_2NH_3^+ + O_2 + H_2O \rightarrow RCHO + NH_4^+ + H_2O_2 \quad (1)$$

CAOs utilize two cofactors during catalysis: a mononuclear, type 2 copper and 2,4,5-trihydroxyphenylalanine quinone (TPQ or TOPA quinone) (*4*). In microorganisms, CAOs enable the amine substrate to be used as a source of carbon and nitrogen during growth. In higher organisms, the enzymes' functions are not well understood, but appear to be involved in physiologically important processes related to the biological role of their natural substrates. For example, polyamines affect the processes of transcription and translation of proteins via interaction with DNA and RNA (*2*). Therefore, the CAOs may regulate fundamental cellular processes such as tissue differentiation, tumor growth, and programmed cell death. One of the reaction products of CAOs, hydrogen peroxide, may also play a role in cell regulation by acting as an intracellular second messenger. It has recently been shown that peroxide can act as a signal-transducing molecule in vascular smooth muscle, evoking responses including tyrosine phosphorylation, MAP kinase stimulation, and DNA synthesis (*5*). In addition, an adhesion protein in both rats and humans which mediates lymphocyte localization has been shown to be a CAO (*6*, *7*). A mechanistically related copper-containing amine oxidase, lysyl oxidase, catalyzes connective tissue maturation by cross-linking elastin and collagen. Its redox cofactor has recently been identified as lysine tyrosylquinone (LTQ), a quinocofactor similar in structure to TPQ in which the side chain of lysine is cross-linked to an oxidatively modified tyrosine (*8*).

In all CAOs studied to date, TPQ is derived posttranslationally from a specific precursor tyrosine (Tyr*) within the protein itself, in a process called biogenesis (*9*). It has been shown in various studies that the protein is capable of processing the precursor residue to TPQ without the aid of exogenous enzymes or cofactors (*10*, *11*). Thus, CAOs are dual-function enzymes, catalyzing both the oxidative deamination of amines in a multiturnover process and the oxygenation of tyrosine to TPQ in a single-turnover event.

From a detailed kinetic study of O_2 utilization during turnover in an amine oxidase from bovine serum (BSAO), it was concluded that the role of the active site copper is to

[†] This work was supported by National Institutes of Health grants to F.S.M. (GM31611) and to J.P.K. (GM39296).

[‡] Crystallographic coordinates have been deposited in the Protein Data Bank under the file name 1EKM.

* Correspondence should be addressed to this author at the Department of Biochemistry and Molecular Biophysics, Washington University School of Medicine, St. Louis, MO 63110. Tel: (314) 362-1080; FAX: (314) 362-7183; email: mathews@biochem.wustl.edu.

[§] Washington University School of Medicine.

[||] University of California, Berkeley.

[⊥] Current address: Research School of Chemistry, Australian National University, Canberra, ACT 0200, Australia.

[#] Current address: Departments of Biological Structure and Biochemistry, Biomolecular Structure Center and Howard Hughes Medical Institute, University of Washington, Seattle, WA 98195.

[1] Abbreviations: *B*-factor, temperature factor; BSAO, bovine serum amine oxidase; CAOs, copper-containing amine oxidases; HPAO, *Hansenula polymorpha* amine oxidase; NCS, noncrystallographic symmetry; RMS, root-mean-square; RMSD, RMS deviation; apoprotein, metal-free and cofactorless protein; apo-Cu, copper-containing but cofactorless HPAO; apo-Zn, zinc-substituted and cofactorless HPAO.

10.1021/bi000639f CCC: $19.00
Published on Web 07/21/2000

stabilize the formation of superoxide anion from O_2 by an electrostatic interaction (*12*). More recent work, in which the metal was removed from a yeast (*Hansenula polymorpha*) copper amine oxidase and replaced with Co^{2+}, provides further support for a nonredox role for copper during turnover (*13*).

In contrast to the effects on catalysis, the presence of copper appears essential for biogenesis. Any replacement of the metal in the apo-protein fails to support TPQ formation (*10*). Recent kinetic and spectroscopic investigations of biogenesis indicate a mechanistically crucial role for the copper, in which a direct ligation between the metal and the precursor tyrosine is formed. This complex is activated toward reaction with molecular oxygen that is prebound at a nonmetal site (*14*, *15*). This proposal extends the hypotheses of previous mechanisms, which had suggested a bimolecular reaction of O_2 with a tyrosine-activated Cu^+ form of the metal (*16*).

Crystallographic results have been obtained for the mature *H. polymorpha* (HPAO) enzyme, as well as amine oxidases from pea seedling (PSAO), *Escherichia coli* (ECAO), and *Arthrobacter globiformis* (AGAO) (*16*−*19*). In addition, an apo-structure has been reported for AGAO (*16*). In the mature, TPQ-containing HPAO enzyme, the cofactor does not directly ligate the active site copper, which is instead coordinated by three histidines and two waters in a roughly square pyramidal geometry (*17*). Interestingly, the structure of the apo-enzyme displayed a reorientation of the precursor tyrosine relative to the mature cofactor, such that the phenolic hydroxyl group was directed toward the vacant metal site (*16*). One interpretation of this result is that the observed reposition supports the assertion that the precursor tyrosine is activated via direct ligation to the metal; however, the absence of a metal in the copper site, together with a structural rearrangement of one of the histidine ligands, limits the use of this structure for detailed mechanistic interpretation.

To avoid these complications, we sought to obtain a structure of the apo-enzyme in which replacement of copper with another metal would result in a more definitive picture of the amine oxidase active site poised for biogenesis. Specifically, zinc was used in an effort to obtain a structure with appropriate residence at the metal site, since it had been previously shown to bind competitively with copper (*20*). Interestingly, not only does this apo-Zn structure display the anticipated ligation of the precursor tyrosine to the metal, but it also elucidates other changes that may help to explain how CAOs are able to carry out dual functions within their active sites.

MATERIALS AND METHODS

Protein Expression and Purification. The zinc-substituted HPAO enzyme was expressed, isolated, and purified as described previously (*20*).

Crystallization. Apo-Zn was crystallized using the wild-type HPAO crystallization protocol employing the hanging-drop vapor-diffusion method with a protein concentration of 12 mg/mL, 9−14% PEG 8000, 100−300 mM potassium phosphate buffer, pH 6.2−7.5, at room temperature for 1 month (*17*). Three crystal forms were obtained under nearly identical conditions. A crystal 0.35 × 0.30 × 0.1 mm^3 in size, belonging to the orthorhombic space group $C222_1$ with unit cell parameters $a = 139.2$ Å, $b = 153.5$ Å, $c = 223.4$ Å, diffracting to 2.4 Å resolution, was used for structure determination. The two other crystal forms belong to the monoclinic space group $P2_1$, with cell constants of $a = 94.6$ Å, $b = 233.0$ Å, $c = 103.9$ Å, $\beta = 91.4°$, and $a = 103.4$ Å, $b = 235.4$ Å, $c = 103.4$ Å, $\beta = 95.0°$, diffracting to 2.8 and 2.6 Å resolution, respectively. The orthorhombic crystal contains three monomers of apo-Zn per asymmetric unit; the value of the Matthews coefficient (*21*) is $V_M = 2.55$ $Å^3$/dalton, which corresponds to a solvent content of 52%.

Table 1: Data Collection and Refinement Statistics

space group	$C222_1$
cell constants (*a*, *b*, *c*; Å)	139.2, 153.5, 223.4
no. of observations	226364
no. of unique reflections	64796
av multiplicity	3.5
R_{merge}[a] (%) 500−2.5 Å/2.6−2.5 Å	8.7/18.5
completeness (%) 500−2.5 Å/2.6−2.5 Å	77.4/40.7
$\langle I/\sigma(I)\rangle$[b] 500−2.5 Å/2.6−2.5 Å	11.8/3.0
resolution range for refinement (Å)	∞−2.5
reflections used for refinement	64455
working set	57931
test set	6524
R_{cryst}[c] (%)	18.3
R_{free}[d] (%)	20.8
no. of non-hydrogen protein atoms[e]	5197
no. of solvent molecules	492
no. of zinc ions[e]	1
RMSD bond lengths (Å)	0.009
RMSD bond angles (deg)	1.69
mean *B*-factor ($Å^2$)	
protein	22.0
solvent	29.4
zinc ions	20.9
RMS Δ*B* (main chain−main chain)	1.1
RMS Δ*B* (main chain−side chain)	1.6
RMS Δ*B* (side chain−side chain)	2.2

[a] $R_{merge} = \Sigma_h\Sigma_i|I(h) - I_i(h)|/\Sigma_h\Sigma_i I_i(h)$, where $I_i(h)$ and $I(h)$ are the *i*th and mean measurements of reflection *h*. [b] $I/\sigma(I)$ is the average signal-to-noise ratio for merged reflection intensities. [c] $R = \Sigma_h|F_o - F_c|/\Sigma_h|F_o|$, where F_o and F_c are the observed and calculated structure factor amplitudes of reflection *h*. [d] R_{free} is the test reflection data set, about 10% selected randomly for cross-validation during crystallographic refinement (*25*). [e] Number of atoms in one independent protomer refined using strict NCS.

Data Collection and Phase Determination. The X-ray diffraction data were recorded to 2.5 Å resolution on an R-axis IV image plate detector using Cu Kα radiation ($\lambda = 1.5418$ Å) from a Rigaku RU-200 rotating anode X-ray generator. The crystal was soaked with 25% glycerol for about 3 min prior to being mounted in a nitrogen gas stream maintained at 110 K. Data were indexed, integrated, and scaled using the HKL package (*22*). Data processing statistics are given in Table 1.

The initial phases for the apo-Zn crystal were obtained by molecular replacement using AMoRe (*23*). The coordinates of monomer A of the wild-type HPAO (PDB accession code 1A2V) were used as the search model. The cross-rotation functions using data from 15 to 5 Å gave an unambiguous orientation for each of the three monomers in the asymmetric unit, with the correct solutions corresponding to the three highest peaks. Clear solutions were also shown in the translation searches. After rigid-body refinement of the three-monomer model, the correlation coefficient was 0.673 and R_{cryst} was 0.316.[2]

Refinement. The model was initially refined in X-plor (*24*) between 10 and 2.6 Å resolution using noncrystallographic symmetry restraints with 10% of the recorded reflections selected randomly for cross-validation using the R_{free} (*25*) and X-ray intensities with $I/\sigma(I) < 1$ omitted.[2] The three copper ions were removed, and the TPQ (residue 405) and the three histidine copper ligands (His456, His458, and His624) in each monomer were changed to alanine in the starting model. Rigid body refinement followed by several rounds of positional and *B*-factor refinement resulted in a lowering of the conventional R_{cryst} and R_{free} to 0.244 and 0.324, respectively. The resulting $2F_o - F_c$ and $F_o - F_c$ electron density difference maps verified that there are three zinc ions in the asymmetric unit, corresponding to the three highest peaks in the $F_o - F_c$ difference map, and Tyr405, His456, His458, and His624 are clearly visible as the zinc ligands in each monomer. Adding the zinc ion and its four ligands to each monomer and manually refitting the model to the electron density using TURBO−FRODO (*26*) on a Silicon Graphics workstation gave $R_{cryst} = 0.222$ and $R_{free} = 0.305$, respectively.

Refinement was then carried out using the program CNS (*27*) with tight noncrystallographic symmetry (NCS) restraints, X-ray intensities less than 0 omitted, and a resolution range between ∞ and 2.5 Å. After positional and *B*-factor refinement, including a bulk-solvent correction (*28*), the residuals were reduced to $R_{cryst} = 0.219$ and $R_{free} = 0.246$. Thereafter, water molecules were added interactively at the end of each refinement cycle. After several iterations of minimization, *B*-factor refinement, bulk-solvent correction, and model refitting, the R_{cryst} and R_{free} were 0.172 and 0.218, respectively. At this point, strict NCS constraints were introduced into the model, thereby reducing the number of crystallographic parameters by a factor of 3 and leaving one independent protomer in the asymmetric unit. This led to final R_{cryst} and R_{free} values of 0.183 and 0.208, respectively, with root-mean-square deviations (RMSD) from ideal values of 0.009 Å for bond lengths and 1.69° for bond angles, respectively. No restraints were applied to the coordination geometry of the zinc ion during the strict NCS-constrained refinement. The final model consists of 1 protomer of apo-Zn HPAO containing 655 amino acids (5197 non-hydrogen protein atoms), 1 zinc ion, and 492 water molecules. The protomer consists of residues 17−672 of the mature protein [residues 16−692 (*20*)] of which the first residue and last 20 residues were disordered. The refinement statistics are summarized in Table 1. The quality of the final model is good as evidenced by electron density difference maps near the zinc site computed using coefficients ($2F_o - F_c$) and ($F_o - F_c$), where F_o and F_c are the observed and calculated structure factors, respectively (Figure 1). The results of PROCHECK (*29*) indicate that 85.0% of the residues are located in the most favorable regions, 14.3% in additional allowed regions, 0.5% in generously allowed regions, and 0.2% in disallowed regions.

RESULTS

Crystal Packing. A major difference between the crystal structure of native HPAO expressed in *S. cerevisiae* and the zinc-substituted HPAO expressed in *E. coli* is the space group symmetry and the crystal packing. The native orthohrombic HPAO crystals are in space group $P2_12_12_1$ with $a = 138.8$ Å, $b = 148.2$ Å, $c = 234.0$ Å (*30*) while the apo-Zn crystals are in space group $C222_1$ with $a = 139.2$ Å, $b = 153.3$ Å, $c = 223.4$ Å. In the native crystals, three molecules of the homodimeric enzyme form a hexamer with 32 point group symmetry within one asymmetric unit. The molecular 3-fold axis is parallel to the crystallographic *a* axis, and a molecular 2-fold axis is tilted ∼12.5° away from the *b* axis in a plane parallel to the *bc* face. In the apo-Zn structure, three homodimeric molecules still pack as a hexamer, but the hexamer is oriented with one of the molecular 2-fold axes coincident with the crystallographic *b* axis while the molecular 3-fold axis is tilted by ∼12.5° from the *a* axis direction in a plane parallel to the *ac* plane. This results in a new packing arrangement between apo-Zn hexamers such that only half the hexamer, i.e., three monomers, makes up the asymmetric unit instead of six monomers as in the native $P2_12_12_1$ cell. Furthermore, this new packing arrangement gives a herringbone pattern to the apo-Zn hexamers when viewed along the crystallographic *b* direction that accounts for the increased *b* axis length and decreased *c* axis length compared to the native HPAO cell. The packing of the three homodimers of HPAO in the hexamer in the two crystal forms is virtually identical. This change in crystal packing may arise from the difference in glycosylation between the mature HPAO, which was expressed in *S. cerevisiae* and contains ∼2% carbohydrate, and the zinc-substituted enzyme expressed in *E. coli*, which contains no carbohydrate.

Structural Differences within the HPAO Molecule. The structure of zinc-substituted HPAO is nearly identical to that of the native copper-containing molecule. When the two homodimers are superimposed, there is ∼0.21 Å RMSD between equivalent C_α positions. Comparison of individual monomers between the two forms results in ∼0.16 Å RMSD, indicating essentially no rearrangement of individual subunits within the dimer.

When individual residues are compared between the two structures, the only significant structural differences are localized to the active site of the enzyme. The largest change occurs at the metal binding site and the site of Tyr405, the precursor to TPQ. Three of the zinc ligands are the same as that of copper in the native HPAO structure: His456 $N^{\epsilon 2}$, His458 $N^{\epsilon 2}$, and His624 $N^{\delta 1}$. However, a new ligand is now formed by Tyr405 $O^{\eta 1}$, which has undergone torsion rotation about the $C^\alpha-C^\beta$ and $C^\beta-C^\delta$ bonds (Figure 1a). The zinc ion is also displaced by about 0.5 Å from the position of the copper ion in the native HPAO structure. The arrangement of the ligands in apo-Zn is nearly tetrahedral (Table 2), with the two water molecules at the axial and equatorial positions in the square pyramidal-coordinated copper of the native enzyme (*17*) being displaced by the Tyr405 ligand.

Two other side chains at the active site are also displaced with respect to the native HPAO (Figure 2a). These are Leu425, which undergoes side chain torsion rotations about its $C^\alpha-C^\beta$ and $C^\beta-C^\gamma$ bonds of ∼120° each, and Met634, which undergoes a rotation about its $C^\gamma-S^\delta$ bond of ∼30°. The remaining side chains in the active site are positioned nearly the same in the two structures.

Variations in Solvent Positions. In Table 2 of Li et al. (*17*), eight active site water molecules are identified which

[2] The quantities R_{merge}, R_{cryst}, and $I/\sigma(I)$ are defined in the footnote of Table 1.

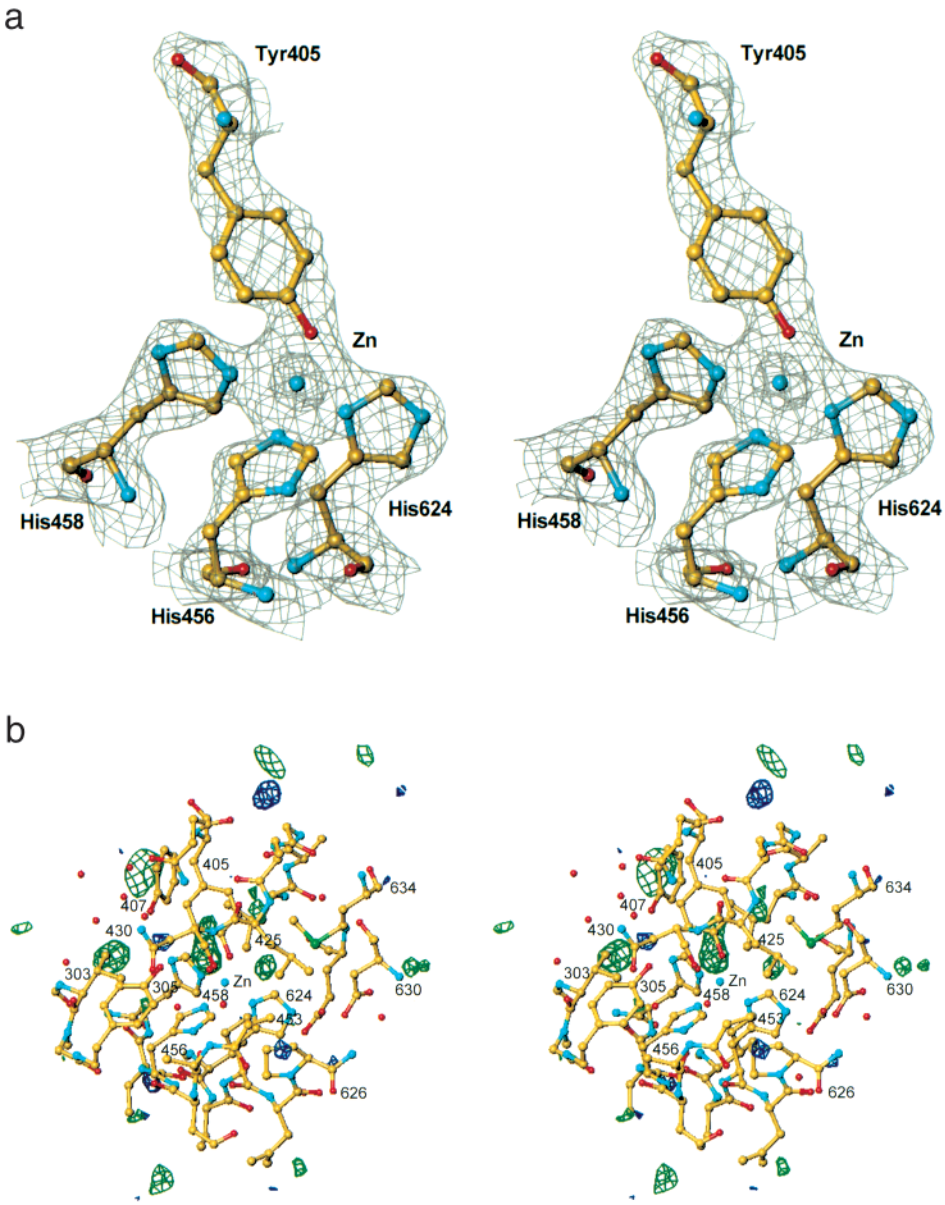

FIGURE 1: Stereo diagrams of the electron density and difference density maps of zinc-substituted HPAO. (a) Coordination of the zinc ion by Tyr405, His456, His458, and His624. This map was computed using coefficients ($2F_o - F_c$), where F_o and F_c are the observed and calculated structure factors, respectively, and the phases are based on the final refined coordinates of the molecular model. The contours are drawn at 1.5 σ and 8 σ, the latter contours surrounding the zinc ion only. (b) Difference electron density, computed using coefficients ($F_o - F_c$), corresponding to the volume within a 10 Å sphere of the zinc ion. Contours are drawn at 3 σ (blue) and -3 σ (green). This diagram was prepared using TURBO−FRODO (*26*).

Table 2: Coordination Geometry of the Zinc Complex of HPAO

ligand (L) atom	Cu−L bond length (Å)	angle (deg) L−Cu−$N^{\epsilon 2}$ (His456)	L−Cu−$N^{\epsilon 2}$ (His458)	L−CuN−$N^{\epsilon 1}$ (His624)
$O^{\eta 1}$ (Tyr405)	2.02	102	119	113
$N^{\epsilon 2}$ (His456)	1.96	–	98	96
$N^{\epsilon 2}$ (His458)	2.08	–	–	120
$N^{\delta 1}$ (His624)	1.89	–	–	–

are generally conserved among the six independent subunits of the native HPAO crystal structure. Two of these, the axial water (Wat_{ax}) and the equatorial water (Wat_{eq}), are bound to the copper and form the fourth and fifth coordination sites of the approximately square pyramidal coordination geometry along with His456, His458, and His 624. A third water molecule, Wat1, is bound to the O-2 position of TPQ and is located in a hydrophobic environment made up of the side chains of Tyr407, Leu425, and Met624. These three waters are displaced in the zinc-substituted HPAO structure. Wat_{ax} and Wat1 are displaced by the Tyr405 side chain coordinated to zinc while Wat_{eq} is displaced by movement of Leu425 (Figure 2b). Waters Wat2 and Wat3 of Li et al. (*17*) link the axial water (Wat_{ax}) of the native HPAO structure to the hydroxyl of Tyr305 and to a solvent-filled channel. Both of these waters are retained in the zinc-substituted HPAO structure, and Wat2 now forms a hydrogen bond bridge between the hydroxyls of Tyr405 and Tyr305 (Figure 2b). Waters Wat4−Wat6 of Li et al. (*17*) are near the substrate binding channel and the site of the reductive half-reaction and may be involved in proton transfer from substrate to product in the overall reaction (*17*). These three waters are also conserved in the zinc-substituted HPAO structure. Two

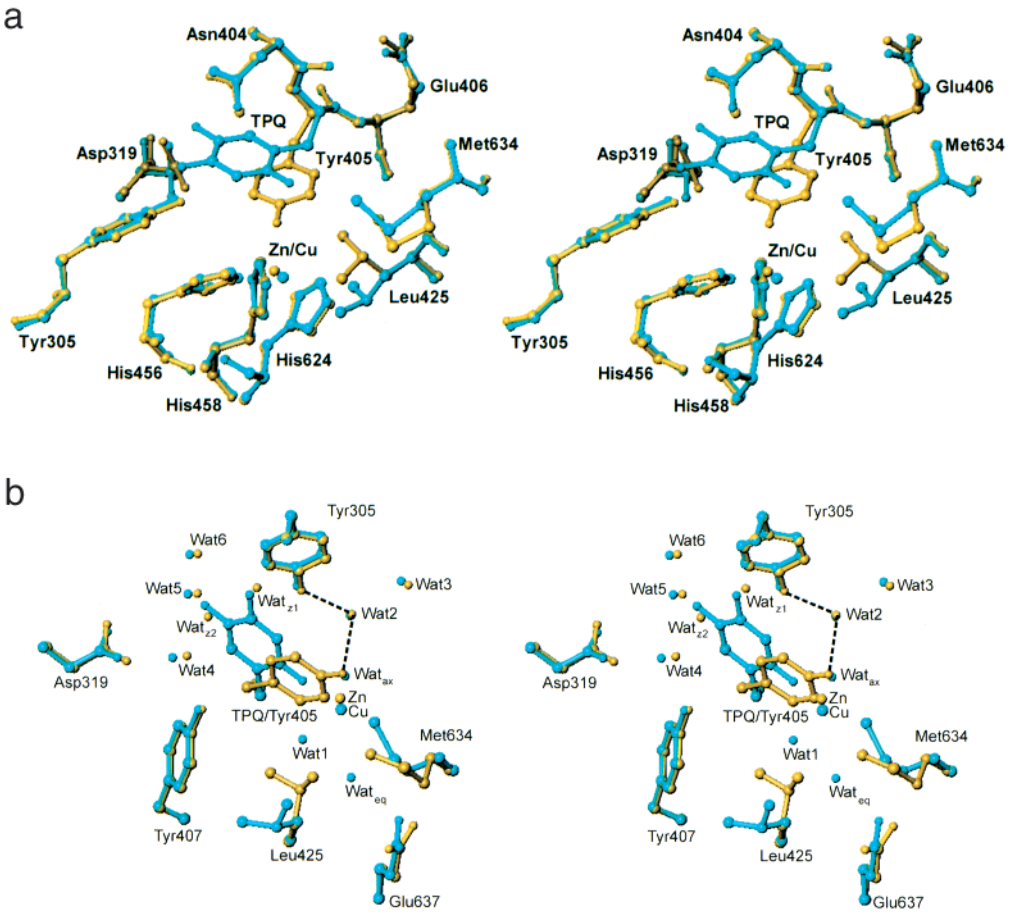

FIGURE 2: Differences in active site conformation in the mature wild-type HPAO (blue) and the zinc-substituted HPAO (yellow). (a) Stereo diagram showing several active site side chains. The only significant side chain movements occur at residues Tyr405 (TPQ), Leu425, and Met624. (b) Stereo diagram comparing the active site water structures as defined in Table 2 of Li et al. (*17*). Waters Wat_{ax}, Wat_{eq}, and Wat1 of mature HPAO have been displaced by Tyr405 and Leu425 in the zinc-substituted enzyme, while waters Wat_{z1} and Wat_{z2} of the zinc-substituted enzyme are displaced by TPQ in the mature enzyme. Waters Wat2−Wat6 are retained in both forms of HPAO, as are most of the internally bound structural waters in the protein. The hydrogen bonds to Wat2 bridging Tyr 305 and Tyr 405 are shown as dashed lines. This diagram was prepared using TURBO−FRODO (*26*).

new water sites, Wat_{z1} and Wat_{z2}, are present in the zinc-containing structure but are displaced by quinone oxygens O-4 and O-5 of TPQ in the mature native structure (Figure 2b).

DISCUSSION

CAOs are unique in that they catalyze two distinct chemical transformations: the oxidative deamination of amines (catalysis) and the conversion of a specific precursor tyrosine to TPQ (cofactor biogenesis) are achieved by this protein. As enzyme active sites are generally regarded as catalysts for a specific transformation, it is of considerable interest how CAOs are able to accomplish both reactions. The catalytic reaction has been the focus of several studies, which have clearly indicated the ping pong mechanism shown in Scheme 1 (*1*). In the first, reductive half-reaction, amine substrate condenses with TPQ to form the substrate Schiff base, followed by deprotonation by an active site aspartate residue to yield the product Schiff base, where the cofactor has been reduced by two electrons. Following hydrolysis and aldehyde release, the reduced cofactor is reoxidized in the oxidative half-reaction. It has been shown that the rate-limiting step in the oxidative half-reaction is the first electron transfer from the reduced cofactor to molecular oxygen, to form superoxide (*12*). Study of the catalytic reaction has been aided by several crystal structures of the mature enzyme (*17*−*19*). In the structure of a phenylhydrazone adduct of ECAO, condensation at the C5 oxygen of TPQ was clearly demonstrated, together with the identity of the active site base and the location of the substrate binding pocket (*31*). From the structure of HPAO, the trafficking of both amines and oxygen into the enzyme was inferred, as was a conserved network of waters implicated in proton equilibration of various intermediates during turnover (*17*).

In contrast to the catalysis, the mechanism of the biogenesis reaction has been less well characterized. Initially it was proposed that the oxygenation of the precursor tyrosine was achieved through activation of O_2, resulting from interaction of molecular oxygen with a reduced form of the active site copper (*16*). However, recent results from detailed spectroscopic and kinetic analyses of biogenesis indicate that the metal serves to activate the precursor tyrosine, such that it can react with prebound O_2 in the key oxygenation step of biogenesis (*14*, *15*).

Contributing to the lack of a definitive mechanism for TPQ formation has been the absence of an appropriate crystal structure. Previously, a structure for the metal-free, apoprotein was reported, where the precursor tyrosine was found to be oriented differently from the mature cofactor, with its

Scheme 1

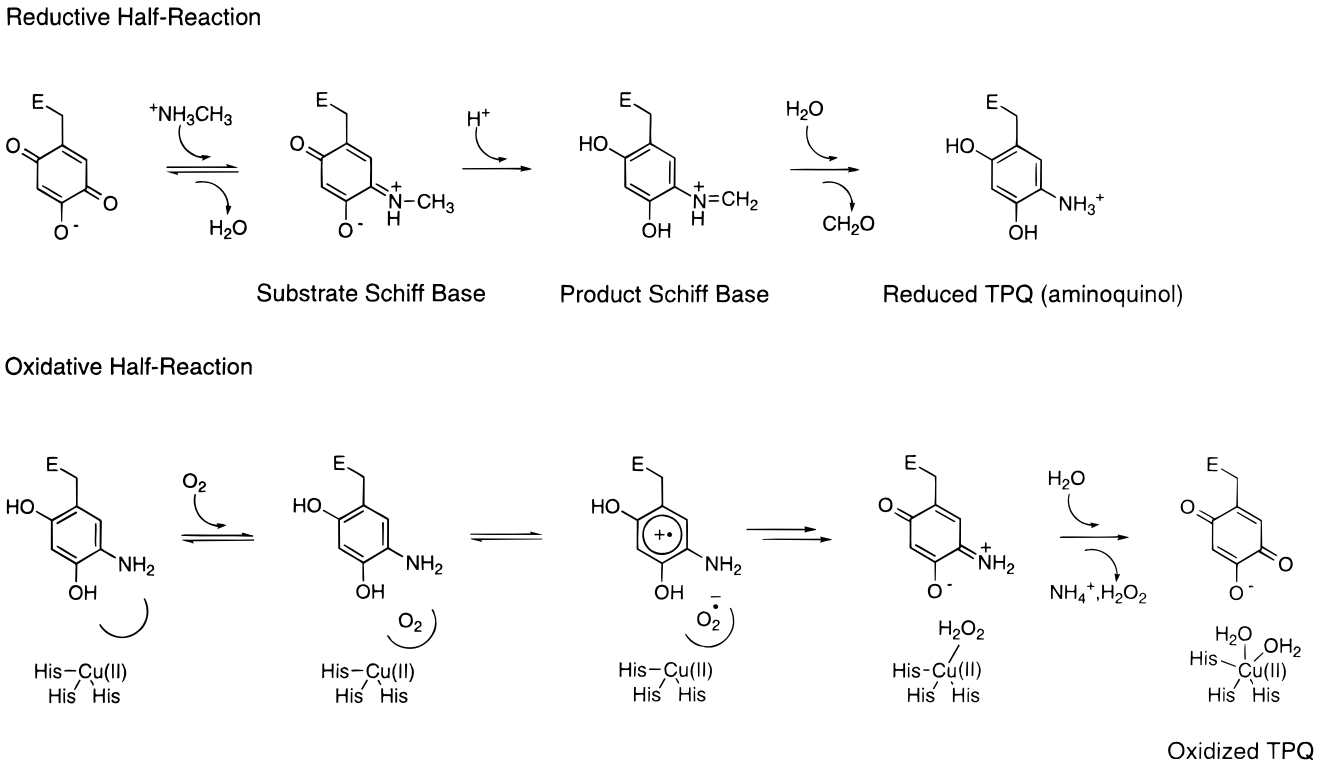

phenolic hydroxyl group pointed toward the vacant metal site (*16*). Though this result supports the proposal of direct activation of the precursor tyrosine, it is difficult to rule out the possibility that the observed structural changes were primarily a result of the absence of metal in the active site. Indeed, not only is the precursor tyrosine observed to move, but also one of the histidines which ligands the copper is found to be reoriented as well, into a configuration which is not expected to be relevant for metal binding.

Thus, we sought a structure of the protein in which the precursor tyrosine was unprocessed to TPQ, but contained a metal present in the active site. It had been previously shown that the presence of zinc can prevent binding of copper by HPAO, and thus prevent formation of TPQ (*20*). The addition of zinc to the apo-protein was expected to produce a suitable structure for envisioning biogenesis, yielding structural changes that could be confidently correlated with mechanistic predictions.

The structure of the zinc-containing enzyme is shown in Figure 1. The zinc is bound at the same site as copper, and is liganded tetrahedrally by three histidines and the precursor tyrosine (Table 2). Importantly, the positioning of the histidine ligands is quite similar to that found in the mature enzyme, supporting the relevancy of this structure. Thus, this structure represents the first snapshot of an amine oxidase poised for cofactor formation.

In terms of mechanistic importance, the most critical feature of the structure is the direct ligation of the precursor tyrosine by the zinc, at a distance of 2.0 Å. Ligation by copper presumably accelerates the oxygenation reaction by inducing radical character on the tyrosine, and thus lowering the kinetic barrier presented by the spin-forbidden nature of this reaction (*32*).

In addition to the reorientation of the precursor tyrosine, several other changes in HPAO are observed to occur, which contrast with the report of the apo-structure. An overlay of the mature HPAO structure with that of apo-Zn reveals that the active site resides Leu425 and Met634 undergo significant movements in their side chains (Figure 2a). During both turnover and biogenesis, it has been proposed that oxygen is bound in an off-metal site prior to chemical reaction (*12*, *15*). In the structure of mature HPAO, three residues, Leu425, Met634, and Tyr407, form a pocket that is found to be weakly occupied by water; based on their hydrophobicity and proximity to TPQ, these residues were proposed to be involved in the binding of O_2 during catalysis (*12*). However, the rearrangement of two of these residues (toward each other) in the apo-Zn structure appears to preclude binding of O_2 in this region during TPQ biogenesis due to spatial occlusion (Figure 2b). Indeed, the two waters found to span these residues in the mature HPAO structure (Wat_{eq} and Wat1) are missing in the apo-Zn enzyme.

Previous studies have shown that the K_m for O_2 during turnover is approximately 15 μM in HPAO, while it is greater than 1 mM during biogenesis (*12*, *15*). Based on the reported lack of conformational change in the active site residues in the apo-structure (*16*), the large change in K_m for O_2 was previously ascribed to a coupling of oxygen binding to motions of the precursor tyrosine (*15*). However, based on the changes observed in the current apo-Zn structure, the change in K_m for O_2 between biogenesis and catalysis may be due to actual physical differences in the binding sites for oxygen.

Though the movements of Leu425 and Met634 preclude oxygen from approaching Tyr405 on one side, the other side of the precursor tyrosine (between Asn404 and Tyr407) appears to be relatively unencumbered and accessible to bulk solvent. In the mature protein, this cavity is occupied by the processed TPQ cofactor; in the apo-Zn structure, the cavity represents an extension of the substrate entry channel

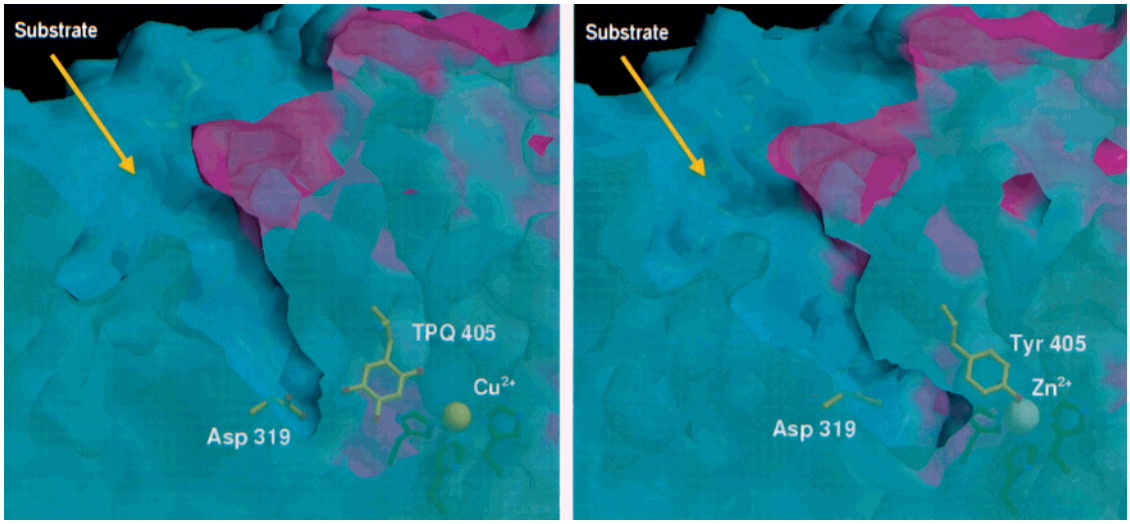

FIGURE 3: Substrate entry channel for HPAO. Left panel: native enzyme showing the TPQ cofactor in its active orientation, below the translucent molecular surface. Also shown are the active site base (Asp319), the copper ion, and its three histidine ligands. Cyan represents one subunit, and violet represents the second subunit. Right panel: apo-Zn enzyme showing the precursor Tyr405 oriented to form a ligand to the zinc ion, thereby extending the substrate channel entry nearly to the metal binding site. Asp319 and the three histidine ligands to the zinc ion are also shown. This diagram was made using GRASP (*37*) and rendered with RASTER3D (*38*).

resulting from reorientation of its tyrosine precursor (Figure 3). An interesting possibility is that Tyr405 initially resides in a similar position to mature TPQ, but that the binding of O_2 to this cavity displaces the precursor tyrosine onto the copper. This idea is supported by recent spectroscopic work by Dove et al., in which a putative tyrosinate−Cu(II) species was observed in the biogeneses of both wild type and a mutant of HPAO, only after the introduction of O_2 to the enzyme (*14*).

The proposed use of the protein channel (Figure 3) by oxygen in the apo-protein and by substrate in mature HPAO is supported by work done by Tanizawa and co-workers, who chemically modified two lysine residues in AGAO (*33*). These amino acids are found to be on the surface of the protein and to reside proximal to the substrate channel; their derivatization resulted in the reduced ability of substrates to access the active site, with a concomitant loss of catalytic activity. However, it was found that in addition to an effect on turnover, the derivatization of these lysines also reduced the rate of TPQ biogenesis. This result does not appear to arise from a chemical role for the lysines, since point mutations of these residues did not affect the rate of biogenesis (*33*). A possible explanation, based on the present structural information, is that occlusion of the substrate channel blocks access of O_2 to the active site of the apo-protein.

A recent structure has been obtained of an amine oxidase from *E. coli*, where a form of oxygen has been trapped on the enzyme during catalysis (*34*). In that study, it was concluded that oxygen was at the peroxide oxidation level, and that it was bound in the axial position of the copper. Though this site may be appropriate for binding of reduced oxygen during turnover, it is viewed as unlikely for the case of biogenesis, since the precursor tyrosine occupies this binding site on the metal.

An additional feature of the structure by Wilmot et al. (*34*) that bears comparison to the apo-Zn structure is the number of ligands to the active site copper. In all structures of resting, oxidized, catalytically competent amine oxidases, the copper is five-coordinate, with two water ligands. As is the case with the apo-Zn structure, the catalytically reduced structure of ECAO shows the metal with only four ligands, the three histidines and peroxide. It appears that both during biogenesis and during catalysis, changes in the ligand field surrounding copper may be crucial for accomplishing the various chemical transformations in amine oxidases. It will be of further interest to determine more accurately how the changes in copper ligation affect reactivity.

An important consideration for this work is that molecular oxygen is not observed to be localized in the proposed binding pocket in the apo-Zn structure. However, to our knowledge the visualization of unreacted O_2 has not been reported in any crystal structure of an enzyme catalyzing monoxygenation, and would probably be difficult to distinguish from water. Even oxygen species expected to be more spatially defined in proteins, such as the iron-associated O_2 in ascaris hemoglobin, generally appear spherical and the oxygen atoms are difficult to resolve, especially adjacent to an electron-dense metal ion (*35*). It will be of great interest for future work to obtain a small molecule which can adequately mimic O_2 in binding to apo-HPAO.

Another consideration is the apparent difference between the kinetic K_m and K_d for binding of oxygen in the apo-protein. If the proposed model for cofactor biogenesis is correct, the binding of O_2 is necessary in order to form the activated Cu−tyrosinate complex. Thus, the observation of this intermediate in the apo-Zn structure implies that under ambient conditions (~0.25 mM O_2) oxygen is almost fully bound; however, the results of a kinetic study of biogenesis indicate that the K_m for oxygen is greater than 1 mM (*15*). There are two possible explanations for this apparent contradiction. The first is that the affinity of apo-Zn HPAO for oxygen may be higher than that of the apo-Cu form. Since the binding of O_2 is coupled to the liganding of Y405, any changes in the affinity of the precursor tyrosine for the metal will affect the K_m observed for oxygen. The second explanation is that the K_m for O_2 is unperturbed in the apo-Zn enzyme, but that its value may be different than the K_d. Since

K_m is a kinetic, rather than thermodynamic, property, its value may be equal to, less than, or greater than the corresponding K_d (*36*).

Finally, in addition to the changes described for specific residues, the overlayed structures of the apo-zinc and mature structures reveal an interesting pattern of water substitutions (Figure 2b). For example, in the apo-Zn structure, two waters (Wat_{z1} and Wat_{z2}) are identified in the area that is occupied by the C4 and C5 oxygens of TPQ in the mature enzyme. These waters are proposed as the site for dioxygen binding during biogenesis, and occupy positions assumed by two of the oxygen atoms on the ring of the mature cofactor. In the latter context, they may be viewed as "placeholders" for oxygen. Similarly, it is noteworthy that the position of the phenolic −OH group in the apo-Zn structure is occupied by a water (Wat_{ax}) in the mature HPAO structure. These differences in the placement of active site waters between the apo- and holo-forms of HPAO may be indicative of a general strategy of amine oxidases to utilize differential solvent-accessible sites as a means of catalyzing dual chemical processes. It will be of general interest to see if this strategy is similarly utilized in other oxidative enzymes containing modified amino acids cofactors, such as galactose oxidase and lysyl oxidase, or if these enzymes require more drastic structural rearrangements to accomplish their dual reactivities.

CONCLUSIONS

The structure of the zinc-substituted apo-HPAO has been solved to 2.5 Å resolution, revealing several key features of TOPA biogenesis in this enzyme. Most importantly, the observation of direct ligation of the precursor tyrosine to the active site metal presents compelling evidence that cofactor formation is initiated by activation of the precursor tyrosine toward reaction with oxygen. This extends a previous hypothesis concerning biogenesis (*16*), and supports more recent conclusions by Klinman and co-workers, who proposed a similar mechanism based on spectroscopic and kinetic results.

In addition to clarifying this key mechanistic question, the apo-Zn structure also suggests that rearrangements of active site amino acid residues may explain observed differences in the kinetic K_m for O_2 during biogenesis and catalysis (*12*, *15*). In particular, rearrangement of residues thought to be involved in binding O_2 to the mature protein precludes access of oxygen to the precursor tyrosine in the apo-protein. However, the movement of the precursor tyrosine itself onto the metal opens up a cavity, which is an extension of the previously identified substrate channel, and provides ready access for O_2. The ability of HPAO to use particular protein elements of channels and bound waters in differential ways is likely the result of the unique requirement of amine oxidases to catalyze both cofactor formation and catalysis.

REFERENCES

1. Klinman, J. P., and Mu, D. (1994) *Annu. Rev. Biochem. 63*, 299−344.
2. McIntire, W. S., and Hartmann, C. (1992) in *Principles and Application of Quinoproteins* (Davidson, V. L., Ed.) pp 97−171, Marcel Dekker, New York.
3. Knowles, P. F., and Dooley, D. M. (1994) *Met. Ions Biol. Syst. 30*, 361−403.
4. Janes, S. M., Mu, D., Wemmer, D., Smith, A. J., Kaur, S., Maltby, D., Burlingame, A. L., and Klinman, J. P. (1990) *Science 248*, 981−987.
5. Sundaresan, M., Yu, Z., Ferrans, V. J., Irani, K., and Finkel, T. (1995) *Science 270*, 296−299.
6. Bono, P., Salmi, M., Smith, D. J., and Jalkanen, S. (1998) *J. Immunol. 161*, 5563−5571.
7. Smith, D. J., Salmi, M., Bono, P., Hellman, J., Leu, T., and Jalkanen, S. (1998) *J. Exp. Med. 188*, 17−27.
8. Wang, S. X., et al., and Klinman, J. P. (1996) *Science 273*, 1078−1084.
9. Janes, S. M., et al., and Klinman, J. P. (1992) *Biochemistry 31*, 12147−12154.
10. Matsuzaki, R., Fukui, T., Sato, H., Ozaki, Y., and Tanizawa, K. (1994) *FEBS Lett. 351*, 360−364.
11. Cai, D., and Klinman, J. P. (1994) *J. Biol. Chem. 269*, 32039−32042.
12. Su, Q., and Klinman, J. P. (1998) *Biochemistry 37*, 12513−12525.
13. Mills, S. A., and Klinman, J. P. (2000) *J. Am. Chem. Soc.* (submitted for publication).
14. Dove, J. E., Schwartz, B., Williams, N. K., and Klinman, J. P. (2000) *Biochemistry 39*, 3690−3698.
15. Schwartz, B., Dove, J. E., and Klinman, J. P. (2000) *Biochemistry 39*, 3699−3707.
16. Wilce, M. C. J., Dooley, D. M., Freeman, H. C., Guss, J. M., Matsunami, H., McIntire, W. S., Ruggiero, C. E., Tanizawa, K., and Yamaguchi, H. (1997) *Biochemistry 36*, 16116−16133.
17. Li, R., Klinman, J. P., and Mathews, F. S. (1998) *Structure 6*, 293−307.
18. Kumar, V., Dooley, D. M., Freeman, H. C., Guss, J. M., Harvey, I., McGuirl, M. A., Wilce, M. C. J., and Zubak, V. M. (1996) *Structure 4*, 943−955.
19. Parsons, M. R., Convery, M. A., Wilmot, C. M., Yadav, K. D. S., Blakeley, V., Corner, A. S., Phillips, S. E. V., McPherson, M. J., and Knowles, P. F. (1995) *Structure 3*, 1171−1184.
20. Cai, D., Williams, N. K., and Klinman, J. P. (1997) *J. Biol. Chem. 272*, 19277−19281.
21. Matthews, B. W. (1968) *J. Mol. Biol. 33*, 491−497.
22. Otwinowski, Z., and Minor, W. (1997) *Methods Enzymol. 276*, 307−326.
23. Navaza, J. (1994) *Acta Crystallogr. A50*, 157−163.
24. Brunger, A. T. (1992) X-PLOR, Version 3.1, Yale University Press, New Haven, CT.
25. Jones, T. A., You, J. Y., Cowan, S. W., and Kjeldgaard, M. (1991) *Acta Crystallogr. A47*, 110−119.
26. Roussel, A., and Cambillau, C. (1991) in *Silicon Graphics Geometry Partners Directory 86*, Silicon Graphics, Mountain View, CA.
27. Brünger, A. T., Adams, P. D., Clore, G. M., DeLano, W. L., Gros, P., Grosse-Kunstleve, R. W., Jiang, J. S., Kuszewski, J., Nilges, M., Pannu, N. S., Read, R. J., Rice, L. M., Simonson, T., and Warren, G. L. (1998) *Acta Crystallogr. D54*, 905−921.
28. Jiang J.-S., and Brunger, A. T. (1994) *J. Mol. Biol. 243*, 100−115.
29. Laskowski, R. A., MacArthur, M. W., Moss, D. S., and Thornton, J. M. (1993) *J. Appl. Crystallogr. 26*, 283−291.
30. Li, R., Chen, L., Cai, D., Klinman, J. P., and Mathews, F. S. (1997) *Acta Crystallogr. D53*, 364−370.
31. Wilmot, C. M., Murray, J. M., Alton, G., Parsons, M. R., Convery, M. A., Blakeley, V., Corner, A. S., Palcic, M. M., Knowles, P. F., McPherson, M. J., and Phillips, S. E. V. (1997) *Biochemistry 36*, 1608−1620.
32. Cox, D. D., and Que, L., Jr. (1988) *J. Am. Chem. Soc. 110*, 8085−8092.
33. Matsuzaki, R., and Tanizawa, K. (1998) *Biochemistry 37*, 13947−13957.
34. Wilmot, C. M., Hajdu, J., McPherson, M. J., Knowles, P. F., and Phillips, S. E. V. (1999) *Science 286*, 1724−1728.

35. Yang, J., Kloek, A. P., Goldberg, D. E., and Mathews, F. S. (1995) *Proc. Natl. Acad. Sci. U.S.A. 92*, 4224−4228.
36. Northrop, D. B. (1998) *J. Chem. Educ. 75*, 1153−1157.
37. Nicholls, A., Sharp, K. A., and Honig, B. (1991) *Proteins*: *Struct., Funct., Genet. 11*, 281−296.
38. Merritt, E. A., and Murphy, M. E. P. (1994) *Acta Crystallogr. D50*, 946−950.

BI000639F